Surface Forces of the Electric Field Induced Flow in Nematic Liquid Crystals

J. Grupp

Physikalisches Institut, Universität Münster

Z. Naturforsch. **39 a,** 309–319 (1984); received December 13, 1983

In thin nematic liquid crystal films with homeotropic boundaries, surface forces are measured that are produced by an electric field induced flow. The sample is placed between two horizontal circular glass disks in a torsion viscosimeter, where a torque is exerted on the upper disk by these surface forces. The evolution of the induced flow is registered via this torque. The time constants of this evolution, the viscosity term $\gamma_1 - \alpha_2^2/\eta_c$ and the elastic constant K_3 are determined.

I. Introduction

In nematic liquid crystal (NLC) films a coupling of the director field and the hydrodynamic flow can occur. Usually the flow is produced by external constraints and the flow alignment of the director field is studied. The inverse effect is also observed: hydrodynamic flow induced by orientational changes [1] (sometimes called backflow [2]). This induced hydrodynamic flow in turn influences the alignment [3]. So the director field behaves in a rather complex manner.

Several investigations deal with the fluid flow that is induced by a change in the director orientation. A direct observation of this flow is – to our knowledge – only reported for the case that a magnetic field is applied to an NLC sample and the flow is observed through the motion of disclinations [4]. In a few investigations of thin NLC films with homogeneous boundaries, the time dependent director field is calculated numerically taking into account the fluid flow [5–7]. From the calculated evolution of the director field the transmissivity of these samples is numerically determined as a function of time. Comparison with calculations that neglect the induced flow show the effect of the fluid motion on the transmissivity. Especially the bounce effect [8] is shown to be caused by the fluid motion.

In our investigations we deal with the fluid flow that is induced by the application of a vertical electric field on an NLC film when the field strength exceeds a critical value. We limit ourselves to the case of homeotropic boundaries and the NLC MBBA having a negative dielectric anisotropy. The MBBA is sandwiched between two parallel circular glass disks of a torsion viscosimeter (Figure 1). The disks are coated with transparent electrically conducting indium-tin-oxid films. The upper (bottom) glass disk is 1 mm (6 mm) thick and 30 mm (46 mm) in diameter. The torsion (upper) disk is suspended by a 30 μm quartz thread coated with a gold film. A more detailed description of the apparatus is given in [9]. In such a torsion shear cell the induced flow is directed tangentially and produces a vertical torque on the torsion disk.

Surface forces are also involved in the hydrodynamic equations of the continuum theory due to Ericksen [10] and Leslie [11]. We employ these equations – similar to Brochard et al. [1] – in the limit of the small angle approximation. The evolution of the director field and the velocity field is calculated from the measured evolution of the torque.

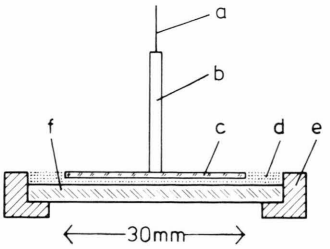

Fig. 1. Scheme of the torsion shear cell: a) quartz thread, b) pin, c) torsion disk, d) NLC, e) socket of f) bottom disk.

Reprint requests to Dr. J. Grupp, Physikalisches Institut, Domagkstr. 75, D-4400 Münster, F.R.Germany.

0340-4811 / 84 / 0400-0309 $ 01.3 0/0. – Please order a reprint rather than making your own copy.

II. Experiments

II.1. Visual observations

We consider a homeotropic aligned sample in the torsion shear cell. The sample appears black when it is placed between crossed polarizers in a monochromatic parallel light beam. Applying a voltage larger than the threshold value U_0 (on an unsheared sample), the Freederickzs transition occurs [12]. The change in the director alignment is seen by the occurrence of concentric interference fringes moving towards the torsion center (Figs. 2b and c). This is very remarkable because with the upper disk fixed one could not observe this high symmetry. Finally – after the orientational change has relaxed – one observes Figure 2d. For this final state Fig. 3b shows schematically the director field in the midplane of the sample using the $\boldsymbol{c}$ director defined in Figure 3a. For symmetry reasons there occurs an umbilic in the torsion center [13].

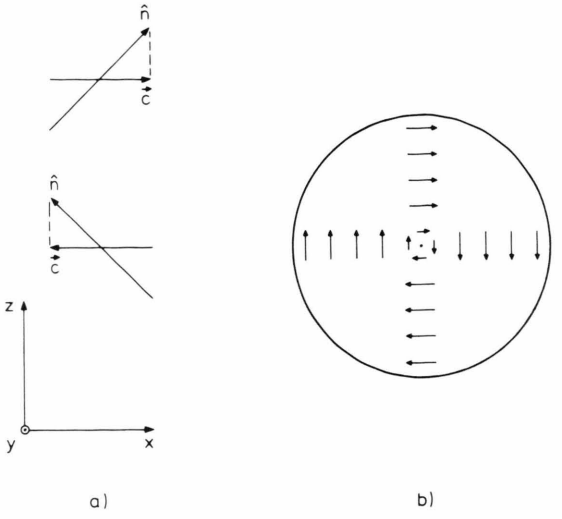

Fig. 3. a) Definition of the $\boldsymbol{c}$ director: projection of the director $\hat{n}$ on the x-y-plane as shown in two examples. b) $\boldsymbol{c}$ directors of the midplane of the sample. The $\boldsymbol{c}$ director field of reverse sign can also occur (see Section II.3.).

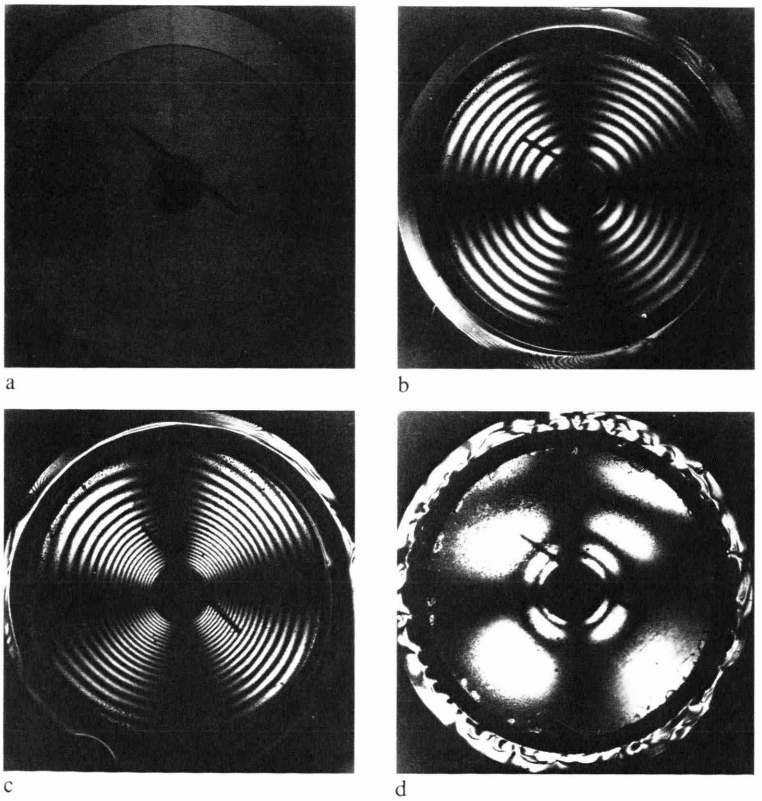

Fig. 2. Photos of the torsion shear cell: a) empty cell, b) a 145 μm thick NLC film placed between crossed polarizers about 50 s after the application of the a.c. voltage (1 kHz) $U = 5.5$ V, c) about 40 s later than b), d) final state.

II.2. Angular motion of the TD

Simultaneously to the optical effects just described a transient angular motion of the torsion disk is observed after the application of the voltage. In Fig. 4a, the corresponding value of the azimuth φ is presented as function of time. The angular motion can be splitted into two parts. The first part is denoted the acceleration process. Here, the angular velocity $\dot{\varphi}\,(\equiv \mathrm{d}\varphi/\mathrm{d}t)$ increases with time. In the second part, $\dot{\varphi}$ decreases and finally equals zero. A (nearly) constant $\varphi(t)$ is reached after a sufficiently long time. This second part is denoted relaxation process. When the applied voltage is switched off a reverse angular motion of the TD is observed (Figure 4b). $\varphi(t)$ approximately reaches the original zero value, when the intermediate small torque of the quartz thread has only caused a negligibly small angular motion. In the presented experiments this holds true because the duration of the field induced flow is very short compared to the relaxation time (of the shear motion) of the torsion disk.

II.3. Direction of the field induced flow

When the direction of the $\boldsymbol{c}$ director of the deformed director field is known a more profound discussion of the orientational change and its related flow is possible. A definite (tangential) direction of the $\boldsymbol{c}$ director can be produced by a torsion shear [14]. The $\boldsymbol{c}$ director field of the midplane of such a sheared sample is similar to Figure 3b.

A suitable shear motion of the torsion disk can be produced by a twist of the quartz thread. In Fig. 5, the full curve shows $\varphi(t)$ measured for a small angle

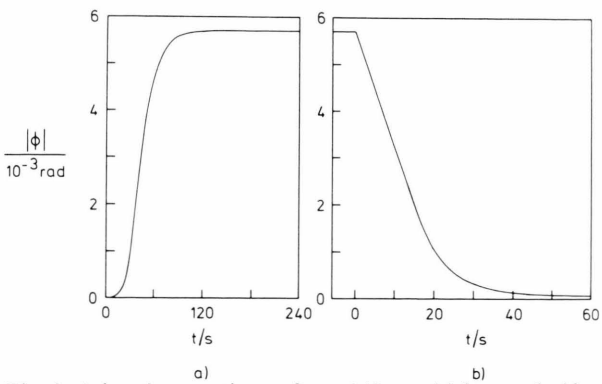

Fig. 4. Azimuth φ vs. time t for a 145 µm thick sample if a) $U = 5.50$ V is applied at $t = 0$. b) $U = 5.50$ V is switched off at $t = 0$.

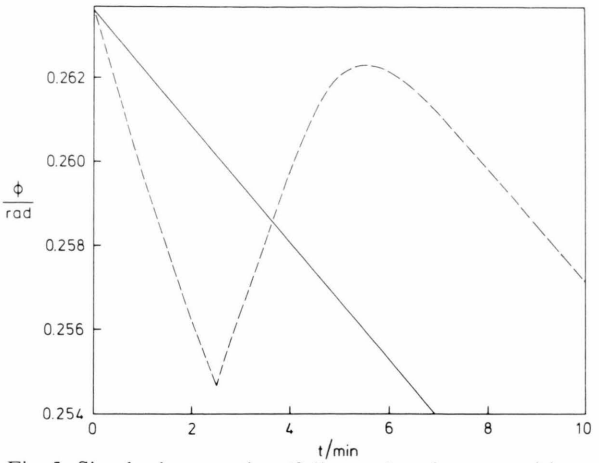

Fig. 5. Simple shear motion (full curve) and superposition (dashed) of a torsion shear motion and a motion that is due to an induced flow (switching off $U = 5.08$ V at $t = 2.5$ min).

interval. The dashed curve shows $\varphi(t)$ when the voltage $U = 5.08$ V has been applied to the sample in addition to the torque of the quartz thread. Here $\varphi(t)$ decreases faster due to the smaller apparent viscosity. At $t = 2.5$ min the voltage is switched off. The flow induced by the orientational change of the director field causes a superposed angular motion which is reversely directed to the original shear motion. When the induced flow has relaxed, the slope of $\varphi(t)$ is the same as that of the full curve.

When an electric field is applied on a sheared sample a flow is produced that affects an angular motion having the same direction as the given shear motion. Such a case is represented in Fig. 6 (see figure caption for details).

These experiments show that the direction of a field induced flow can be determined by the sign of a given shear motion. Taking into account simultaneous optical observations (Part II.1) it is obvious that the induced flow is uniformly tangential in the shear cell.

Let us now discuss the observed phenomena for a linear shear cell (Figure 7). An applied force $\boldsymbol{F}_s$ shifts the upper boundary with a velocity $\boldsymbol{v}_s$. In Fig. 7a, the director field is shown as formed by such a given shear. The resulting $\boldsymbol{c}$ director points into the same direction as the velocity $\boldsymbol{v}_s$. Application of a voltage will increase the deformation angle ψ and the $\boldsymbol{c}$ director (Fig. 7c) inducing a flow as is schematically presented in Fig. 7b (see for example

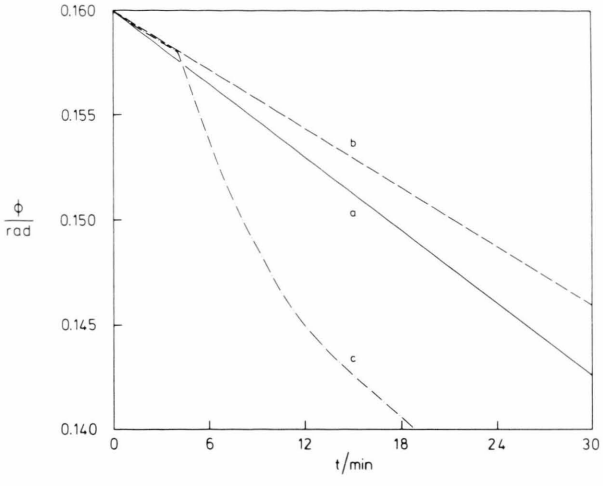

Fig. 6. Superposition of a torsion shear motion and a motion due to an electric field induced flow. Curve a represents the shear with $U = 4.31$ V applied and curve b without an applied voltage. Curve c shows the shear under no voltage in the first place. At $t = 4$ min, $U = 4.31$ V is applied. When the field induced flow has relaxed (at about 17 min) the curve c has the same slope as the curve a.

[2]). The experiments (Fig. 6) have shown that applying a voltage increases the angular velocity of the torsion disk. This means the surface force $\boldsymbol{F}_f$ due to the field induced flow points into the same direction as the external force $\boldsymbol{F}_s$ and into the opposite direction of the flow velocity of the boundary zone. This can be explained in a simple manner: The field induced flow stems from the boundaries by exerting a force ($\boldsymbol{F}_f$) that is oppositely directed to the flow velocity in the boundary zone according to Newton's law (actio = reactio).

In Fig. 7d, the case is represented where a voltage is switched off. Here, the deformation of the director field (Fig. 7c) is reduced inducing a flow with a velocity field that is reversed compared to the application of an electric field. Therefore the force that is caused by the rotation of the director field is also reversed. This means the force $\boldsymbol{F}_f$ and the external force $\boldsymbol{F}_s$ are oppositely directed. If $\boldsymbol{F}_f$ is larger than $\boldsymbol{F}_s$ the boundary is shifted oppositely to $\boldsymbol{F}_s$ (see Figure 5).

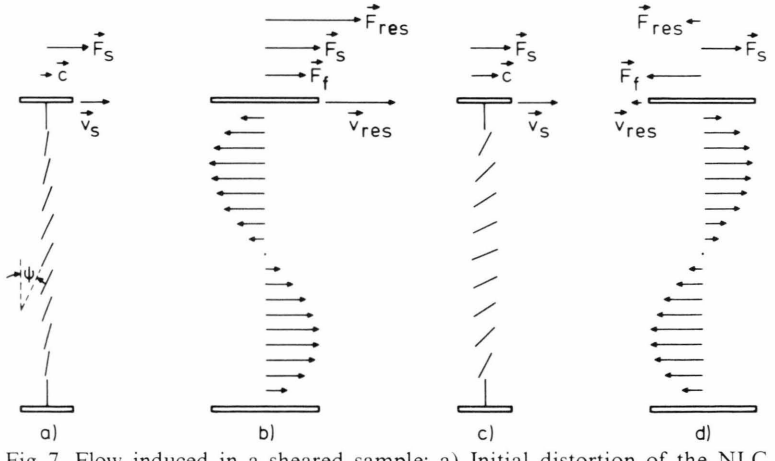

Fig. 7. Flow induced in a sheared sample: a) Initial distortion of the NLC produced by the external shear. b) Schematic presentation of a momentary velocity field of the electric field induced flow. The related surface force $\boldsymbol{F}_f$ and the external force $\boldsymbol{F}_s$ add up to the total surface force $\boldsymbol{F}_{res}$ acting on the upper boundary. The motion of the boundary is indicated by $\boldsymbol{v}_{res}$. c) Deformation structure under an applied voltage after the electric field induced flow has relaxed. Due to the smaller apparent viscosity, $\boldsymbol{v}_s$ is here larger than in a). d) Flow induced by switching off the voltage (transition from c) to a)). The force $\boldsymbol{F}_f$ is oppositely directed to the $\boldsymbol{c}$ director, respectively $\boldsymbol{F}_s$.

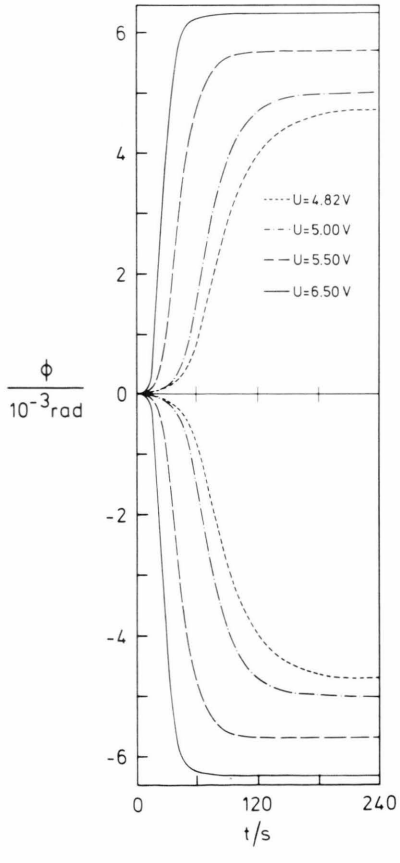

Fig. 8. Angular motions of the torsion disk for different voltages applied at $t = 0$. For each applied voltage angular motions of both signs are possible ($d = 145$ μm).

When a superposed shear motion is absent the direction of the induced flow is observed to be also tangential. The magnitude of the rotation of the torsion disk is always equal for the application of a fixed voltage but the sign of the rotation is unpredictable. In a series of experimental runs, rotations of positive and negative signs (Fig. 8) are observed (if distortions of the homeotropic boundaries are absent). This can be explained as follows: when an overcritical electric field is applied the Freederickzs transition is induced by fluctuations of the director orientation [15]. This means that the onset in the director field deformation takes place locally. In the torsion shear cell, however, the first onset of director reorientation exerts a force on the torsion disk. If the tangential component of this force causes a small angular motion of the disk a coherent deformation of the whole director field is induced. So the flow of the whole sample becomes uniformly parallel to the tangential direction.

II.4. Birefringence

In most of the former investigations the birefringence or the transmissivity was used to study the dynamics of NLC films that are subjected to external fields. We have performed similar experiments. As described in Part II.1 interference fringes move to the torsion center after an overcritical voltage has been applied. The local interference order is measured by use of the narrow beam of a He-Ne-laser. The light beam penetrates the sample at a distance r from the torsion center. The transmissivity is detected by a photodiode. In Fig. 9, the signal $S(t)$ of the photodiode is shown as a function of time after a voltage of 4.6 V has been switched on or off. The corresponding rotation angle $\varphi(t)$ is also shown. In Fig. 10, the order of the interference fringe $N(t)$ is presented for two different detector positions: $r_1 \approx 6$ mm $(N_1(t))$ and $r_2 = 13$ mm $(N_2(t))$. Here a voltage of $U = 7.0$ V is applied at $t = 0$. It can be seen that there is a time shift Δt between the two detector signals concerning the same order N. It is obvious that the mechanical measure is more sensitive to the initial orientational change. Using the order N, the maximal distortion angle ψ^* of the director field is estimated for the end of the acceleration process: $\psi^* \approx 2 \cdot 10^{-2}$ rad. This means that the acceleration process is related to very small distortion angles.

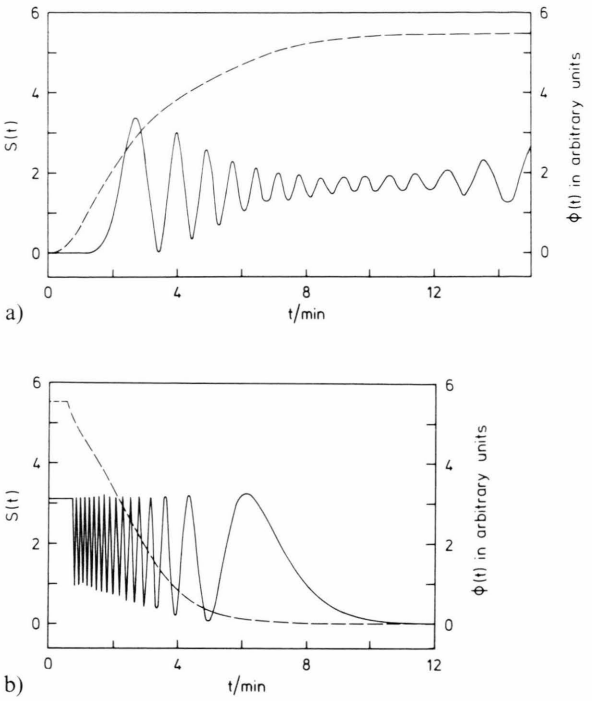

Fig. 9. $S(t)$ (full curve) and $\varphi(t)$ (dashed) of a 159 µm thick sample when a) $U = 4.60$ V is applied at $t = 0$, b) $U = 4.60$ V is switched off at $t = 0.7$ min.

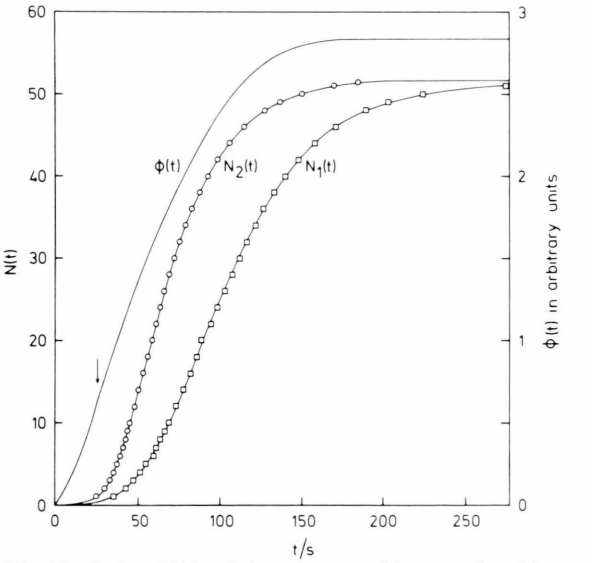

Fig. 10. Order $N(t)$ of interference fringe and $\varphi(t)$ as function of time ($U = 7.0$ V, $d = 159$ µm). Here, the end of the acceleration process is indicated by an arrow. For technical reasons the sample is subjected to a tiny torsion shear before the voltage is applied at $t = 0$.

III. Theory

In the following we only consider the acceleration process. The hydrodynamic equations of the NLC are solved for this process in the small angle approximation. First the electric field induced flow is treated assuming a linear shear cell. The results obtained are subsequently transformed to the tangential flow in the torsion shear cell. This is allowed because inertial forces can be neglected.

III.1. Hydrodynamic equations in the small angle approximation

According to the continuum theory of Ericksen and Leslie [10, 11] the equations for the velocity field $\boldsymbol{v}$ and the director field $\hat{n}$ of NLC are

$$\varrho \dot{v}_i = F_i + t_{ij,j}\,, \tag{1}$$

$$\varrho_1 \ddot{n}_i = G_i + g_i + s_{ij,j} \tag{2}$$

with the constraints

$$v_{i,i} = 0, \quad n_i n_i = 1\,. \tag{3}$$

Subscripts i and j denote the Cartesian coordinates, the j succeeding the comma denotes differentiation with respect to the j-th coordinate and summation over repeated indices has to be carried out. The first equation represents the conservation of linear momentum, ϱ denoting the density, $\boldsymbol{F}$ any external body force and $\mathbf{t}$ the stress tensor. The second equation is equivalent to the conservation of angular momentum. ϱ_1 is a molecular inertial coefficient, $\boldsymbol{G}$ a generalized body force, $\boldsymbol{g}$ a generalized intrinsic body force and $\mathbf{s}$ a generalized stress tensor. The inertial terms in (1) and (2) can be neglected [6]. The body force $\boldsymbol{F}$ (e.g. due to space charges) is negligibly small in our case. Therefore (1) reduces to

$$t_{ij,j} = 0\,. \tag{1a}$$

The geometrical situation studied is schematically shown in Figure 11. The generalized body force G_i arises here from the electric field $\boldsymbol{E}$ [6]:

$$G_x = 0\,, \quad G_y = \Delta\varepsilon\, E^2 n_x\,, \quad G_z = 0\,. \tag{4}$$

$\boldsymbol{E}$ is parallel to the z-axis and $\Delta\varepsilon$ denotes the value of the dielectric anisotropy. The velocity and director field subject to the boundary conditions

$$\begin{aligned} &n_x(\pm d/2) = 0\,, \quad n_y \equiv 0\,, \quad n_z(\pm d/2) = 1\,, \\ &v_x(\pm d/2) = 0\,, \quad v_y \equiv 0\,, \quad v_z \equiv 0\,. \end{aligned} \tag{5}$$

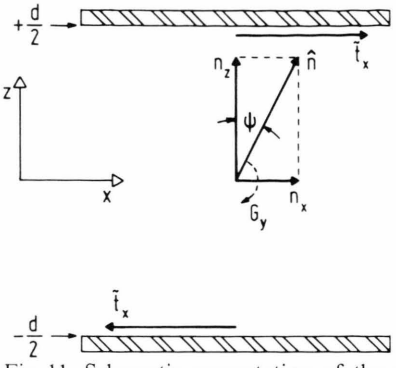

Fig. 11. Schematic presentation of the geometry studied. The electric field is parallel to the z-axis and tends to increase the deformation angle ψ as is indicated. The components $\tilde{t}_x$ of the surface forces are related to the transient flow that arises when a voltage is applied on the initial homeotropic structure (similar to Figure 7b).

For small distortions the director field can be approximated by

$$\hat{n} \approx (\psi(z), 0, 1)\,. \tag{6}$$

The dynamic contribution $\tilde{t}_{xz}$ to the component t_{xz} of the stress tensor [11] is in the small angle approximation

$$\tilde{t}_{xz} = \eta_c v_{x,z} + \alpha_2 (\partial\psi/\partial t)\,, \tag{7}$$

where η_c is a viscosity coefficient according to Miesowicz [16]. In this approximation we obtain from (1a) and (2):

$$\frac{\partial}{\partial z}\left(\eta_c v_{x,z} + \alpha_2 \frac{\partial\psi}{\partial t}\right) = 0\,, \tag{8a}$$

$$\Delta\varepsilon E^2 \psi + K_3 \frac{\partial^2\psi}{\partial z^2} - \gamma_1 \frac{\partial\psi}{\partial t} - \alpha_2 v_{x,z} = 0\,. \tag{8b}$$

K_3 is the elastic bend constant [17] and γ_1 is a viscosity coefficient [11]. A trial solution of ψ satisfying the boundary conditions is

$$\psi = \psi_0 \cos(\pi z/d) \exp(t/\tau_a)\,. \tag{9}$$

Here the space dependent factor corresponds to the static solution of (8b) [15]. This approximation differs from the dynamic solution of the hydrodynamic equations given by Brochard et al. [1]. The validity of our solution will be discussed below (Section V). The exponential time dependence is stimulated by the exponential increase of the angle $\varphi(t)$ (see for example Figure 12). Taking into

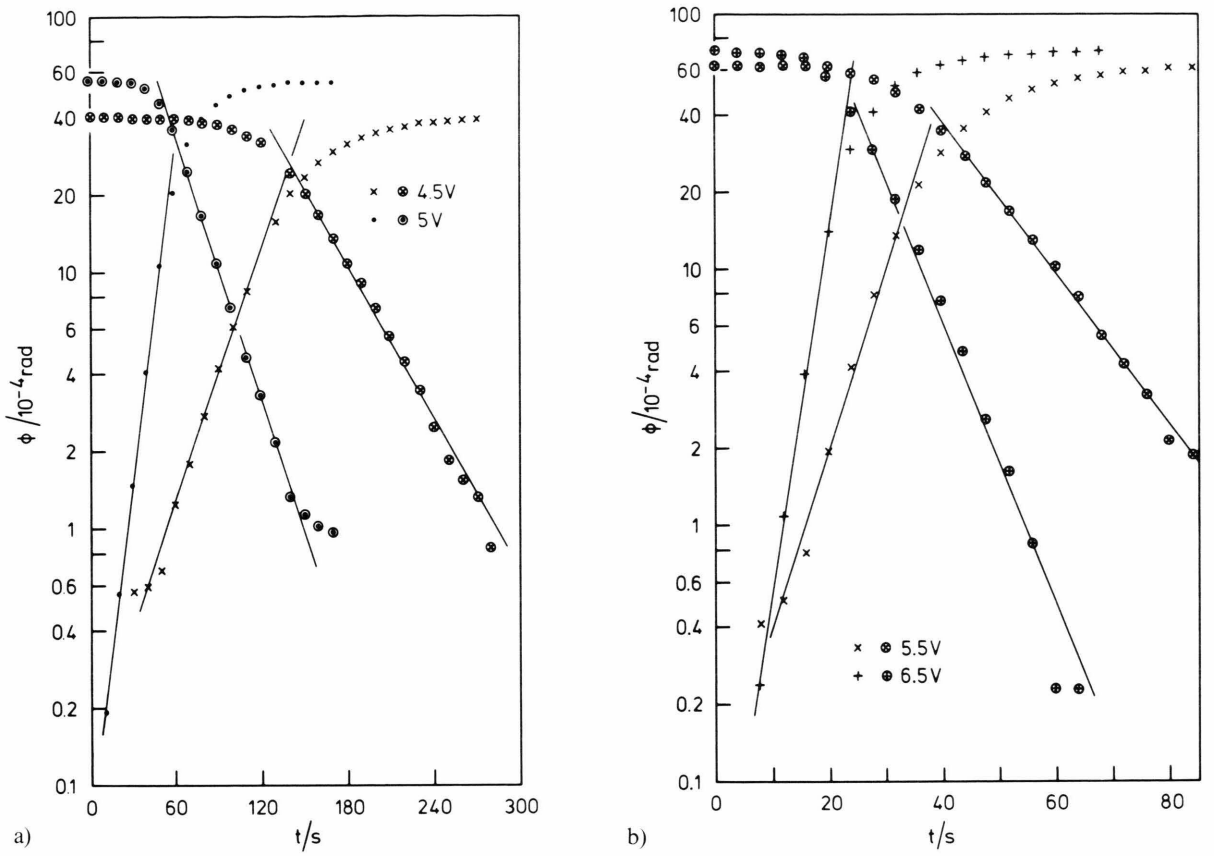

Fig. 12. Azimuth φ on a logarithmic scale presented as function of the time t, if a voltage is applied at $t = 0$. The function $\varphi_m - \varphi(t)$ is also shown on the same scale for each voltage (encircled points).

account the boundary conditions (5) and employing the solution (9) we obtain from (8a) by integration:

$$v_x(z,t) = \alpha_2 \psi_0 d (\eta_c \tau_a \pi)^{-1} \cdot [2z/d - \sin(\pi z/d)] \exp(t/\tau_a) . \tag{10}$$

When $v_{x,z}$ is substituted in (8a) by using (8b) the following condition is obtained for the time constant τ_a:

$$\tau_a^{-1} = C (U^2 - U_0^2) ,$$

where

$$C = \Delta\varepsilon/d^2 (\gamma_1 - \alpha_2^2/\eta_c) \tag{12}$$

and

$$U_0 = (K_3/\Delta\varepsilon)^{1/2} . \tag{13}$$

U_0 is the threshold voltage of the Freedericksz transition.

III.2. Surface forces in a linear shear cell

The dynamical tangential surface force per unit area $\tilde{t}$ of an NLC is: $\tilde{t} = \tilde{\mathbf{t}} \hat{f}$ [18]. Here $\hat{f}$ is the unit vector of the surface. According to Landau and Lifschitz [19] $\hat{f}$ points outwards from the fluid when the external force on the surface of the liquid is considered. When the force is considered which is exerted on the solid boundaries by the fluid, $\hat{f}$ is taken to pointing into the fluid. In our experiments we deal with the surface force on the upper boundary ($z = +d/2$, Fig. 11): $f_z = -1$. Using (9) and (10) we obtain from (7):

$$\tilde{t}_x = -2\alpha_2 \psi_0 (\pi \tau_a)^{-1} \exp(t/\tau_a) . \tag{14}$$

III.3. Surface forces in the torsion shear cell

As the field induced flow occurs tangentially in our torsion viscosimeter the results for the linear

shear cell can easily be extended to the torsion shear cell ignoring centrifugal forces. Hereto we replace $\tilde{t}_x$ by $\tilde{t}_\varphi$. The forces that are exerted on a surface element $2\pi r\,dr$ of the torsion disk, produce a contribution $M_r = 2\pi \tilde{t}_\varphi r^2\,dr$ to the torque on the disk. The value of the total torque is obtained by integration ($R \equiv$ radius of the disk):

$$M = \tfrac{2}{3}\pi \tilde{t}_\varphi R^3 . \tag{15}$$

Inserting (14) yields

$$M = -\tfrac{4}{3} R^3 \alpha_2 \psi_0 \tau_a^{-1} \exp(t/\tau_a) . \tag{16}$$

The angular motion of the torsion disk can be described by the balance of torques [9]:

$$J\ddot{\varphi} + k\dot{\varphi} + D\varphi = M . \tag{17}$$

J is the moment of inertia, k the friction coefficient of the disk, D the torsion coefficient of the quartz thread and M the torque due to the field induced flow that is given by (16). In the acceleration process the torque M is mainly balanced by the torque due to the inertia of the torsion disk because φ remains very small and $J\ddot{\varphi} \gg k\dot{\varphi}$:

$$J\ddot{\varphi} \approx M . \tag{18}$$

By this a solution for φ is implied involving the time constant τ_a of (16): $\varphi = \varphi_0 \exp(t/\tau_a)$. Using (16) we obtain from (18)

$$\psi_0 = -3\varphi_0 J/(4\alpha_2 \tau_a R^3) . \tag{19}$$

The quantities on the right side are either constants or available by measurements. Equation (19) is inserted into (14) ($\tilde{t}_x \to \tilde{t}_\varphi$):

$$\tilde{t}_\varphi = 3J\varphi_0 (2\pi \tau_a^2 R^3)^{-1} \exp(t/\tau_a) . \tag{20}$$

This equation is used to determine the surface force due to the field induced flow. τ_a and φ_0 are obtained for each applied voltage from the angular motion of the torsion disk.

IV. Results

As an example the results of experiments on a 145 µm thick sample with the clearing point $T_c = 40.3\,°C$ are presented. In the following we write φ instead of $|\varphi|$.

Figure 12 shows the angular motion of the torsion disk for different applied voltages. For each voltage two curves are shown: $\varphi(t)$ and $\varphi_m - \varphi(t)$. φ_m is the final azimuth that is reached when the flow has relaxed. Evidently the angular motion can be approximated by two exponentials

$$\varphi(t) = \varphi_0 \exp(t/\tau_a) \quad \text{for} \quad 0 < t < t_c ,$$
$$\varphi_m - \varphi(t) = \varphi_1 \exp(-t/\tau_d) \quad \text{for} \quad t > t_c ,$$

corresponding to the acceleration and the relaxation process. τ_a and τ_d are presented in Fig. 13 as functions of the applied voltage. Both curves show a hyperbolic shape. According to (11), τ_a^{-1} is plotted vs. U^2 in Figure 14. From the slope of the obtained straight line the bend viscosity term (see for example de Gennes [20]) $\eta_B = \gamma_1 - \alpha_2^2/\eta_c$ is obtained

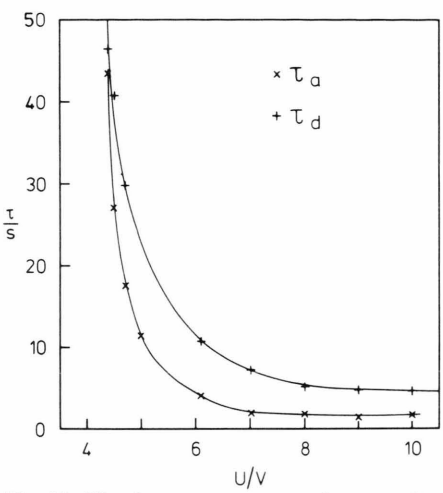

Fig. 13. The time constants τ_a and τ_d vs. voltage U.

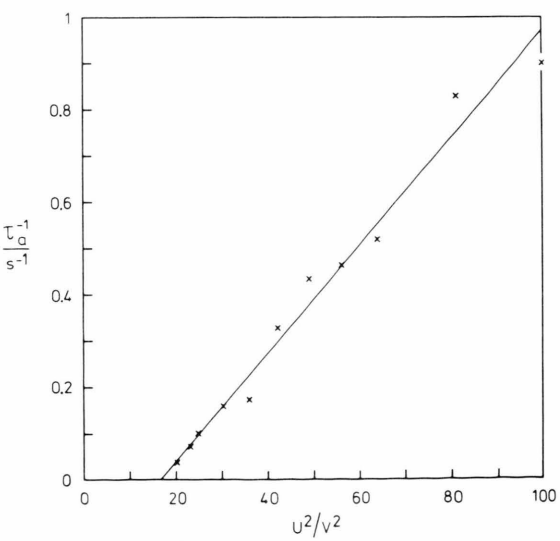

Fig. 14. τ_a^{-1} vs. U^2.

using $\Delta\varepsilon$ from Klingbiel et al. [21] in (12): $\eta_B = 0.0184\ \mathrm{Nsm^{-2}}$ at $T = 25.6\ ^\circ\mathrm{C}$ [22]. The involved sample thickness d has been determined from capacitance measurements performed on the homeotropic sample [9]. Calculating η_B from the viscosity coefficients measured at $T = 25\ ^\circ\mathrm{C}$ by Gähwiller [23] one obtains $\eta_B = 0.0181\ \mathrm{Nsm^{-2}}$. Using the results (at $T = 25\ ^\circ\mathrm{C}$) of Kneppe et al. [24], $\eta_B = 0.0194\ \mathrm{Nsm^{-2}}$ is obtained. Our experimental results agree satisfactorily with these values. In Fig. 14, a threshold voltage $U_0 = 4.01$ V of the Freederickzs transition is obtained from the extrapolation of the straight line to $\tau_a^{-1} = 0$. Using (13) the elastic constant K_3 is determined from this value: $K_3 = (7.4 \pm 0.4) \cdot 10^{-12}$ N. This constant is also in agreement with those from other authors (see for example de Gennes [20]).

The angular motion of the torsion disk indicates that the surface force $\tilde{t}_x$ ($|\tilde{t}_\varphi| \equiv |\tilde{t}_x|$) due to the field induced flow reaches a maximal value $\tilde{t}_x^{\max}$ at about the end of the acceleration process ($t_c \approx 6.5\ \tau_a$). The local amplitude of the flow velocity $v_{x0}(t)$ also reaches roughly its maximal value $v_{x0}^{\max}$ at the time $t = t_c$. In Fig. 15, $\tilde{t}_x^{\max}$ and $v_{x0}^{\max}$ are shown as functions of the applied voltage U. In the investigated range of U, both the quantities increase exponentially with U.

In Fig. 16, the angular motion of the torsion disk is shown for two voltages that are switched off at $t = 0$. Except for a short initial acceleration, the angle φ decreases exponentially with time. The time constants for the exponential decay are approximately equal for all voltages used.

V. Discussion

The analysis of the field induced flow has been performed in the small angle approximation that is valid for the acceleration process since the deformation angle of the director field remains very small (below $\approx 10^{-2}$ rad). The evolution of the director field is described by using the quasi-static

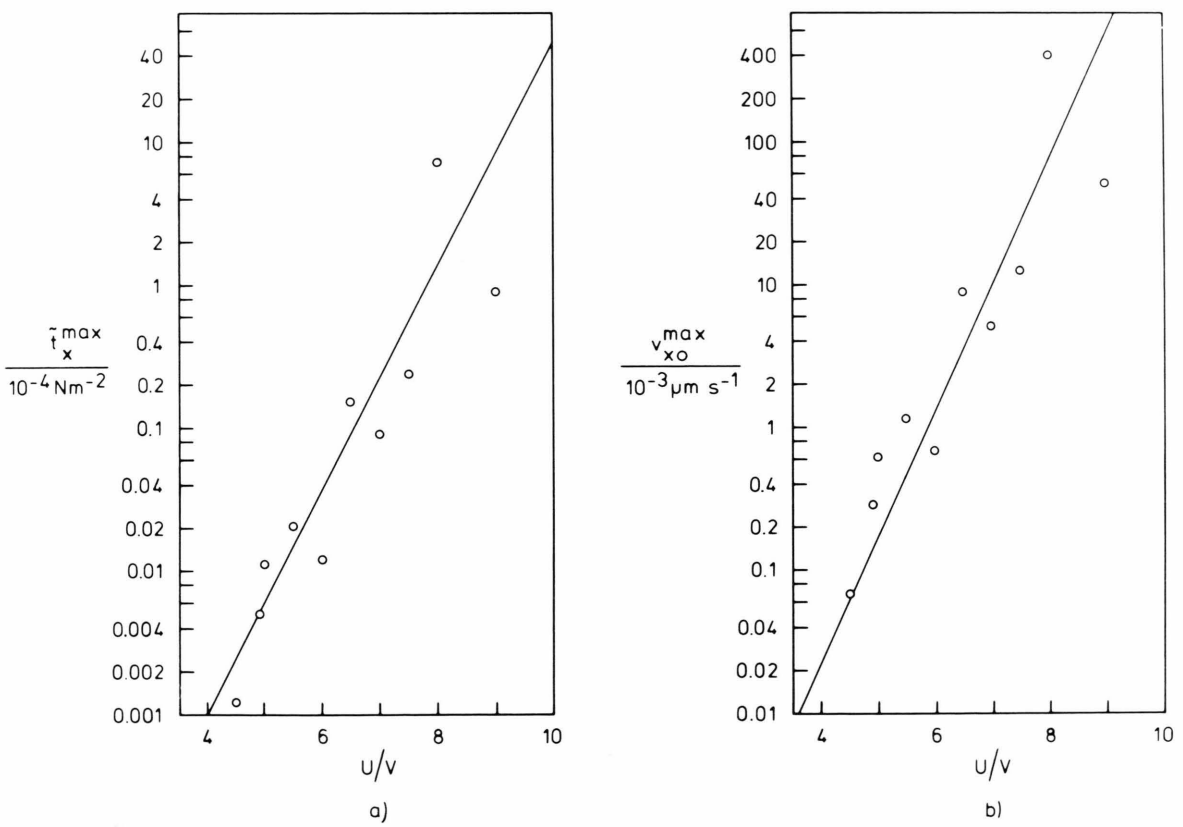

Fig. 15. a) $\tilde{t}_x^{\max}$ and b) $v_{xo}^{\max}$ vs. voltage U.

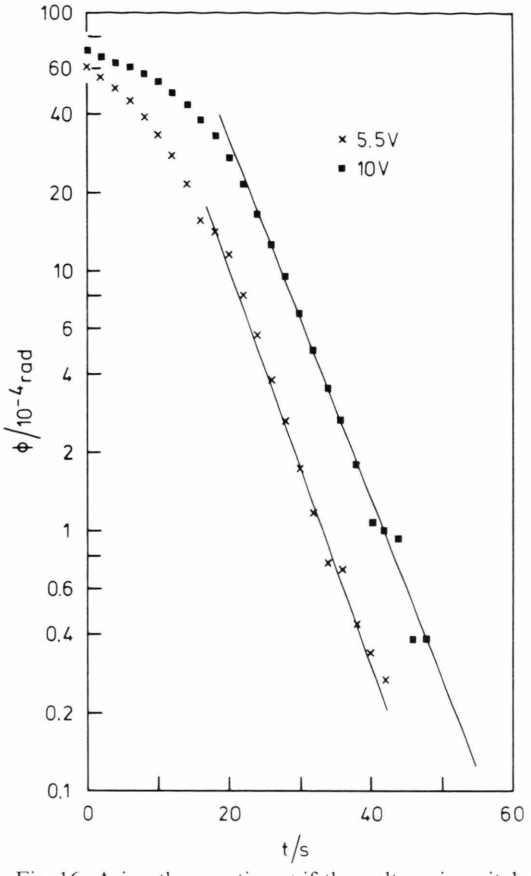

Fig. 16. Azimuth φ vs. time t if the voltage is switched off at $t = 0$.

solution which is correct since the measured time constants obey (11) in the investigated voltage range.

The angular motion of the torsion disk certainly influences the evolution of the field induced flow. In the case of the acceleration process this influence can be neglected. In the relaxation process this feedback can become large. Further, the feedback depends on the radius r as is indicated by the motion of the interference fringes in the optical image. By changing the experimental conditions the rotation of the torsion disk can be reduced. So by using a thicker quartz thread the feedback could be suppressed to a large extent.

The pure electric field induced flow can only be investigated in a voltage range that is limited by the threshold level U_0 of the Freederickzs transition and the critical level U_c for the onset of electrohydrodynamic (EHD) convection. In the case of the sample described in Chapt. IV, these values are $U_0 = 4.01$ V and $U_c = 10.5$ V when an a.c. voltage of 1 kHz is applied. Beyond the critical voltage a periodic oscillatory angular motion of the torsion disk is observed that is due to EHD convection. This phenomenon is already described elsewhere [25].

In our considerations we have neglected the influence (feedback) of the field induced flow on the director orientation. This is certainly allowed in the case of smaller applied voltages and of thin films of nematics because here the field induced flow is weaker and the related viscous torques are negligibly small in comparison to the electric and elastic torques. In the case of larger applied voltages this is also true for the initial flow (acceleration process). At the end of the acceleration process, however, an additional deformation of the director field can be produced by the viscous torques that must not be neglected. Such phenomena are the subject of current investigations.

Acknowledgements

Many useful discussions with Prof. Dr. F. Fischer are gratefully acknowledged. I want to thank R. Arends for making the drawings. Part of the results was presented at the Bunsen-Kolloquium on "Materialeigenschaften und Ordnungszustände von Flüssigkristallen" in Berlin in 1983.

[1] F. Brochard, P. Pieranski, and E. Guyon, Phys. Rev. Lett. **28,** 1681 (1973).
[2] S. Chandrasekhar, Liquid Crystals, University Press, Cambridge 1977.
[3] M. G. Clark and F. M. Leslie, Proc. Roy. Soc. London **A 361,** 463 (1978)
[4] L. Léger, Sol. State Comm. **10,** 697 (1972).
[5] C. Z. van Doorn, J. Phys. (Paris) **33,** C 1–261 (1975).
[6] C. Z. van Doorn, J. Appl. Phys. **46,** 3738 (1975).
[7] D. W. Berreman, J. Appl. Phys. **46,** 3746 (1975).
[8] C. J. Gerritsma, C. Z. van Doorn, and P. van Zanten, Phys. Lett. **A 48,** 263 (1974).
[9] J. Grupp, Rev. Sci. Instrum. **54,** 754 (1983).
[10] J. L. Ericksen, Trans. Soc. Rheol. **5,** 23 (1961).
[11] F. M. Leslie, Arch. ration Mech. Analysis **28,** 265 (1968).
[12] V. Freederickzs and V. Tsvetkov, Phys. Z. d. Sowjetunion **6,** 490 (1934).
[13] F. Fischer, J. Wahl, and Th. Waltermann, Ber. Bunsenges. Phys. Chem. **78,** 891 (1974).
[14] J. Wahl, Z. Naturforsch. **34 a,** 818 (1979).
[15] Pieranski, F. Brochard, and E. Guyon, J. Phys. Paris **34,** 35 (1973).
[16] M. Miesowicz, Nature London **17,** 261 (1935).

[17] F. C. Frank, Disc. Faraday Soc. **25,** 19 (1958).
[18] F. M. Leslie, Adv. Liq. Cryst. **4,** 1 (1979).
[19] L. D. Landau and E. M. Lifschitz, Hydrodynamik, Lehrbuch der Theoretischen Physik VI, Akademie-Verlag, Berlin 1966.
[20] P. G. de Gennes, The Physics of Liquid Crystals, Clarendon, Oxford 1974.
[21] R. T. Klingbiel, D. J. Genova, and H. K. Bücher, Mol. Cryst. Liq. Cryst. **27,** 1 (1973).
[22] This value differs slightly form that given by the author in his Ph.D. Dissertation, Münster 1981, owing to a calibration error.
[23] Ch. Gähwiller, Phys. Lett. **A 36,** 311 (1971).
[24] H. Kneppe, F. Schneider, and N. K. Sharma, J. Chem. Phys. **77,** 3203 (1982).
[25] J. Grupp, Sol. State Commun. **44,** 627 (1982).